J. Fluid Mech. (1985), vol. 157, pp. 199–224
Printed in Great Britain

On a submerged sphere in a viscous fluid excited by small-amplitude periodic motions

By S. A. JENKINS AND D. L. INMAN
Center for Coastal Studies, University of California, San Diego, La Jolla, CA 92093

(Received 12 December 1983 and in revised form 18 December 1984)

Higher-order nonlinear corrections to the Stokes pendulum problem are calculated in perturbation schemes for small values of Reynolds numbers $R^{(2)} = u_m d_0/2\nu$. Here the controlling lengthscale $\frac{1}{2}d_0$ is the displacement amplitude of the undisturbed periodic motion, u_m is the velocity amplitude and ν is the kinematic viscosity. Solutions for two general types of periodic motion are found; namely orbital motion as under deep water waves and oscillatory motion as under shallow water or acoustic waves. These solutions are found by matched asymptotic expansions using the fundamental irrotational oscillation to drive a thin Stokes a.c. boundary layer over the surface of the sphere. From the boundary layer several secondary motions are excited which die away in the neighbouring fluid. Among these are an orthogonal system of steady, rotational Eulerian streaming currents, and two outwardly radiating non-dispersive waves, one having the frequency of the fundamental but with a phase shift, the other appearing at the second harmonic.

With these solutions the forces and torques on a fixed sphere were computed. One of the orthogonal components of the rotational streaming field was found to produce a rotary lift force which opposed virtual-mass forces and diminished the resultant force component in quadrature to the fundamental oscillation. The other streaming component contributed damping terms which, unlike leading-order Stokes drag, vary nonlinearly with the displacement amplitude. Steady and second-harmonic torques were found to act on the sphere about the horizontal axis transverse to the fundamental oscillation.

1. Introduction

This paper finds an analytic approximation for the motion near a sphere in the middle of a column of water while linearized gravity waves progress over the surface with phase speed $c = \sigma/k$. The radian frequency of these monochromatic waves is σ and k is the wavenumber = 2π/wavelength. The diameter d_0 of free-particle orbits at the depth $\frac{1}{2}h$ of the sphere will be small with respect to the sphere diameter $D = 2a$. Because the waves are of small steepness ϵ the sphere radius remains small relative to the incident wave length, $ka \ll 1$. The problem has thus been simplified physically, since diffraction effects and flow separation remain undeveloped.

The solution herein by matched asymptotic expansions is equivalent at lowest order to the Stokes pendulum (Stokes 1851). It proceeds to higher orders in figure 1 following a linear analysis introduced by Schlichting (1932) and later extended to water waves by Longuet-Higgins (1953, 1970), Hunt & Johns (1963) and Lamour & Mei (1977). It is well known that this linear analysis is subject to some rather restrictive assumptions. The severest of these is the low-Reynolds-number form of

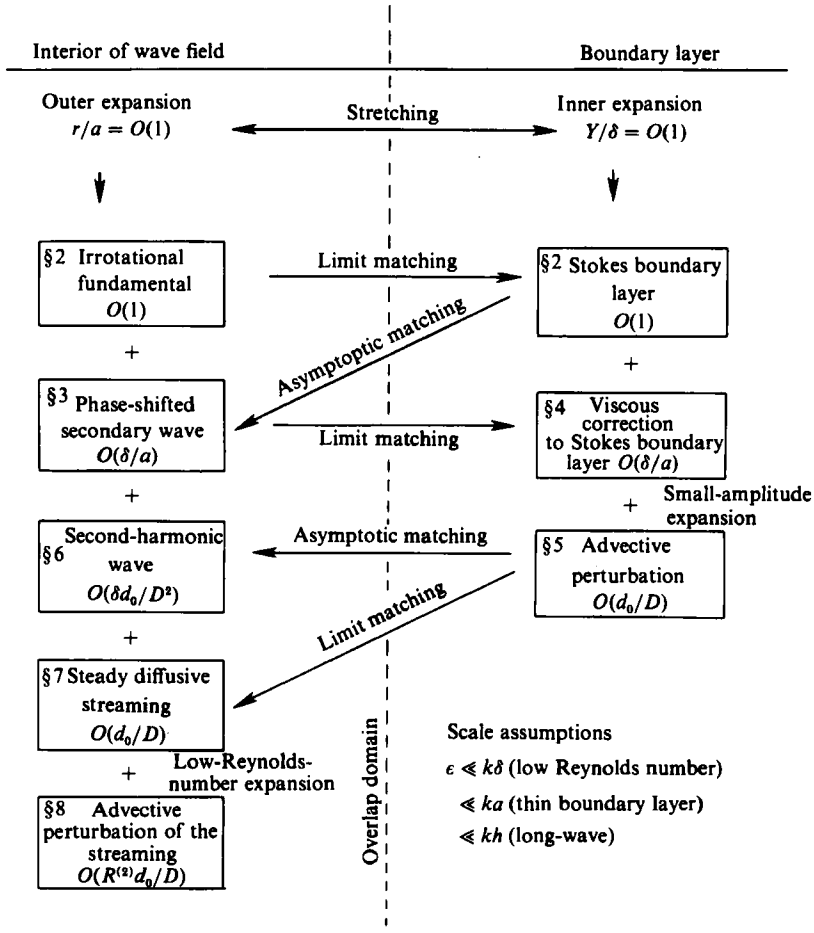

FIGURE 1. Matching diagram for the solution to a sphere under a linearized wave by matched asymptotic expansions.

the small-amplitude assumption, $R^{(2)} \ll 1$. Here the amplitude of the fundamental oscillation, $\frac{1}{2}d_0 = u_m/\sigma$, must remain small not just relative to the body, but small relative to an already thin boundary layer,

$$\delta = O[(2\nu/\sigma)^{\frac{1}{2}}], \quad \text{or}$$

$$R^{(2)} = u_m d_0/2\nu = d_0^2/2\delta^2 \ll 1.$$

In addition, any rotational corrections generated through the linear analysis are assumed not to interact with the irrotational fundamental oscillation, as supported by arguments in Riley (1965). The linear analysis assumes that some final steady state exists and neglects all transients by considering the problem at some time, $t \to \infty$, long after the initiation of motion.

We have pursued linear analysis herein to show that the fully three-dimensional diffusive solutions, when $R^{(2)} \to 0$, are sufficiently well behaved at great distances to yield advective corrections to the rotational field outside the periodic boundary layer. This was not accomplished in the more singular two-dimensional or planar problems cited above. These advective corrections for small yet non-vanishing Reynolds

numbers are of interest because they produce torques and nonlinear corrections to the wave forces as well as suggest the birth of certain high-Reynolds-number flow features like those calculated numerically by Duck & Smith (1979).

2. Formulation

Certain preferred coordinate systems will give great savings in labour when solving for the motion near a fixed submerged sphere. The primary coordinate system to which the incident waves and the resultant forces on the sphere are referenced is the Cartesian system $(\hat{x}, \hat{y}, \hat{z})$ with the origin at the centre of the sphere, midway between the free surface and a plane flat bottom. In this system the axis ox is positive in the direction of the group velocity, the axis oz is positive vertically upward, while the axis oy is positive transversely in a left-handed system. Since the local boundary conditions are with respect to a spherical surface, it will be easier to prescribe motions within a few radii of the sphere in terms of the spherical polar coordinates $(\hat{r}, \theta, \alpha)$. Here $\hat{r}$ is the dimensional radial coordinate measured from the centre of the sphere, θ is the polar angle about the x-axis and α is the azimuth angle measured from oz to a projection of the radius vector in the (y, z)-plane.

A number of forced higher-order solutions found in following sections have either axisymmetry or concentricity with respect to the horizontal transverse axis oy. Work on these solutions is simplified with respect to a Cartesian frame $(\hat{x}', \hat{y}', \hat{z}')$ obtained by rotating the primary system $(\hat{x}, \hat{y}, \hat{z})$ by $\frac{1}{2}\pi$ around the vertical axis. The spherical polar coordinates relative to the rotated system are $(\hat{r}, \theta', \alpha')$. The transformation between the primary and rotated coordinates is given by

$$\left.\begin{aligned} \hat{x}' = \hat{y} &= \hat{r}\cos\theta' = \hat{r}\sin\theta\sin\alpha, \\ \hat{y}' = -\hat{x} &= \hat{r}\sin\theta'\sin\alpha' = -\hat{r}\cos\theta, \\ \hat{z}' = \hat{z} &= \hat{r}\sin\theta'\cos\alpha' = \hat{r}\sin\theta\cos\alpha. \end{aligned}\right\} \tag{2.1}$$

Boundary-layer solutions will be developed in a thin spherical shell and lend themselves to description in curvilinear coordinates $(\hat{X}, \hat{Y}, \hat{Z})$ or $(\hat{X}', \hat{Y}', \hat{Z}')$. The unprimed system has its origin fixed to the surface of the sphere at $\theta = 0$. The axis OY is normal to the spherical surface, while OX and OZ are the axes tangential to the surface along arcs of longitude and latitude respectively. The primed curvilinear system has the same arrangement about its origin at $\theta' = 0$. The coordinate transformations from the curvilinear to the spherical polar system are

$$\hat{X} = a\theta, \quad \hat{Y} = \hat{r} - a, \quad \hat{Z} = a\alpha\sin\theta, \tag{2.2}$$

$$\hat{X}' = a\theta', \quad \hat{Y}' = \hat{r} - a, \quad \hat{Z}' = a\alpha'\sin\theta'. \tag{2.3}$$

The previous studies of Stokes (1851), Schlichting (1932) and Longuet-Higgins (1970) took the undisturbed fundamental oscillation to be uniform. The undisturbed wave oscillation from classical linearized theory (Lamb 1932, chap. 9) may also be approximated as a uniform flow in the neighbourhood of $\hat{r}/a \to O(1)$ by the following expansion:

$$\left.\begin{aligned} \hat{\phi}_\infty &= u_m x\cos\sigma t - w_m z\sin\sigma t + O(ka), \\ \hat{\boldsymbol{u}}_\infty &= \boldsymbol{\nabla}\hat{\phi}_\infty, \\ u_m &= \tfrac{1}{2}\sigma d_0, \quad w_m = \tfrac{1}{2}\sigma d_0\tanh\tfrac{1}{2}kh, \\ d_0 &= H\frac{\cosh\frac{1}{2}kh}{\sinh kh}. \end{aligned}\right\} \tag{2.4}$$

where

This error can be made acceptably small while still imposing the necessary small-amplitude assumptions if the wave steepness $\epsilon = \frac{1}{2}kH$ is further constrained according to

$$\epsilon \frac{\cosh \frac{1}{2}kh}{\sinh kh} < k\delta < ka < \begin{cases} kh & (kh \leqslant 1), \\ 1 & (kh > 1). \end{cases} \tag{2.5}$$

The first inequality in (2.5) is the low-Reynolds-number assumption, $R^{(2)} \ll 1$; the second is the thin-boundary-layer approximation, $\delta/a \ll 1$, the last is the long-wavelength limit, $ka \ll 1$, for a finite depth.

In order to neglect the effects of compressibility on the velocity distribution (Batchelor 1967), we shall require that the frequency of the wave oscillation be sufficiently small such that

$$\sigma d_0/2\tilde{c} \ll 1, \tag{2.6}$$

where $\tilde{c}$ is the speed of sound in the fluid.

From these scale assumptions take $(u_m, a, 1/\sigma)$ as the characteristic velocity, length- and timescales for the fluid motion outside the periodic boundary layer. Using the convention of writing dimensional variables with hats (^), we define the following $O(1)$ non-dimensional outer variables in the near field:

$$\boldsymbol{u} = \frac{\hat{\boldsymbol{u}}}{u_m}, \quad t = \sigma \hat{t}, \quad r = \frac{\hat{r}}{a}, \quad p = \frac{\hat{p}}{\rho \sigma u_m a}. \tag{2.7}$$

The non-dimensionalization of variables by (2.7) will decompose the Navier–Stokes equation outside the boundary layer into a system of ordered linear equations by seeking an expansion for the velocity as

$$\boldsymbol{u} = \nabla\phi^{(1)} + \frac{\delta}{a}\nabla\phi^{(2)} + \frac{\delta d_0}{D^2}\nabla\phi^{(3)} + \frac{d_0}{D}\langle \boldsymbol{u}^{(3)} \rangle. \tag{2.8}$$

The irrotational fundamental oscillation $\phi^{(1)}$ consists of the undisturbed incident wave ϕ_∞, from (2.4), and a scattered wave ϕ_s. The long-wavelength limit, $ka \ll 1$, to the inviscid scattering problem can be found from solutions by Rayleigh (1876) for a sphere in plane shallow water or acoustic-type waves, and by Havelock (1954) for a spheroid of arbitrary eccentricity either at rest or translating under deep-water waves. For a stationary sphere, both solutions can be reduced over the near field, $r = O(1)$, to the form

$$\left.\begin{aligned} \phi^{(1)} &= \phi_\infty + \phi_s = \phi_\infty \left(1 + \frac{1}{2}\,\frac{1}{r^3}\right), \\ \boldsymbol{u}^{(1)} &= \nabla\phi^{(1)}. \end{aligned}\right\} \tag{2.9}$$

Thus diffraction effects leading to local shadows or bright spots do not appear, as the scattered wave spreads energy uniformly in all directions.

While the condition of vanishing normal flow at the surface of the sphere is met by the potential scattering solution (2.9), the no-slip condition cannot be satisfied, since

$$\lim_{r\to 1}\left[\frac{1}{r}\,\frac{\partial\phi^{(1)}}{\partial\theta}\right] = u_{\theta_0}^{(1)} = \mathrm{Re}\left\{\mathrm{i}\,\frac{3}{2}\left[C\,\mathrm{e}^{\mathrm{i}(\theta+t)} - D\,\mathrm{e}^{-\mathrm{i}(\theta-t)}\right]\right\}, \tag{2.10}$$

$$\lim_{r\to 1}\left[\frac{1}{r\sin\theta}\,\frac{\partial\phi^{(1)}}{\partial\alpha}\right] = u_{\alpha_0}^{(1)} = \mathrm{Re}\left\{\tfrac{3}{2}E_0\,\mathrm{e}^{\mathrm{i}t}\right\}, \tag{2.11}$$

where
$$C = \tfrac{1}{2}[1 + \tanh \tfrac{1}{2}kh \cos\alpha],$$
$$D = \tfrac{1}{2}[1 - \tanh \tfrac{1}{2}kh \cos\alpha],$$
$$E_0 = -\mathrm{i} \sin\alpha,$$

and Re means 'take the real part'.

Equations (2.10) and (2.11) show that the fundamental oscillation near the sphere consists of a pair of waves concentric with the transverse axis oy and a third component wave having axisymmetry about oy. The concentric motion is a mixed standing–progressive oscillation, separable into two component waves of amplitudes C and D, progressing in opposite directions around each vertical slice, α = constant. The axisymmetric wave is a purely standing oscillation with complex amplitude E_0, and is everywhere orthogonal to the two concentric component waves. These non-vanishing circumferential velocities over the curved surface of the sphere produce centrifugal forces manifested as circumferential pressure gradients. These pressure gradients will drive the Stokes boundary layer, where ultimately the no-slip condition is satisfied.

To satisfy the no-slip condition there must exist a region of non-uniformity near the sphere where the scaling (2.7) of outer variables, leading to negligible viscous terms, becomes invalid. To retain the viscous terms it may be inferred that the thickness of this region must be $O(\delta/a)$. Hence we define the $O(1)$ inner (boundary-layer) variables:

$$\left.\begin{aligned} &X = \frac{\hat{X}}{a}, \quad Z = \frac{\hat{Z}}{a}, \quad Y = \frac{(\hat{r}-a)}{a\Delta}, \quad \Delta = \frac{\delta}{a}, \quad U = \frac{\hat{U}}{u_{\mathrm{m}}}, \\ &W = \frac{\hat{W}}{u_{\mathrm{m}} \tanh \tfrac{1}{2}kh}, \quad V = \frac{\hat{V}}{u_{\mathrm{m}} \Delta}, \quad P = \frac{\hat{P}}{\rho\sigma u_{\mathrm{m}} a}, \quad t = \sigma\hat{t}, \end{aligned}\right\} \tag{2.12}$$

where $(\hat{U}, \hat{W}, \hat{V})$ are the dimensional tangential and normal velocity components of $\boldsymbol{U}$ corresponding to $(\hat{u}_\theta, \hat{u}_\alpha, \hat{u}_r)$ respectively. The Navier–Stokes equations for the boundary layer in terms of dimensionless variables according to (2.12) are reducible to a system of ordered linear equations taking component expansions in the following scheme:

$$\left.\begin{aligned} U &= U^{(1)} + \frac{\delta}{a} U^{(2)} + \frac{d_0}{D} U^{(3)} + O\left(\frac{\delta^2}{a^2}\right), \\ V &= V^{(1)} + \frac{\delta}{a} V^{(2)} + \frac{d_0}{D} V^{(3)} + O\left(\frac{\delta^2}{a^2}\right), \\ W &= W^{(1)} + \frac{\delta}{a} W^{(2)} + \frac{d_0}{D} W^{(3)} + O\left(\frac{\delta^2}{a^2}\right). \end{aligned}\right\} \tag{2.13}$$

The lowest-order solution in this scheme is the Stokes a.c. boundary layer on a sphere (Lamb 1932, Art. 347), and may be written as

$$U^{(1)} = \zeta' u_{\theta 0}^{(1)}, \quad W^{(1)} = \zeta' u_{\alpha 0}^{(1)}, \quad V^{(1)} = -2\zeta \frac{\partial u_{\theta 0}^{(1)}}{\partial\theta}. \tag{2.14}$$

The primed functions are derivatives with respect to Y, where

$$\zeta' = 1 - \mathrm{e}^{-(1+\mathrm{i})Y}, \quad \zeta = Y + \frac{1}{1+\mathrm{i}} \mathrm{e}^{-(1+\mathrm{i})Y} - \frac{1-\mathrm{i}}{2}. \tag{2.15}$$

The tangential oscillations of the Stokes boundary-layer limit match with fundamental irrotational oscillations at the outer edge of the boundary layer, (2.10) and (2.11). The boundary-layer oscillations normal to the sphere do not match with the fundamental oscillation in the limit sense.

3. Phase-shifted secondary oscillation

In attempting the matching, it was learned that the outer edge of the Stokes boundary layer vibrates with a normal velocity distribution $u_{r0}^{(2)}$ given as

$$u_{r0}^{(2)} \equiv \lim_{r\to 1} u_r^{(2)} = (1-\mathrm{i})\,\frac{\partial u_\theta^{(1)}}{\partial \theta}. \tag{3.1}$$

This motion is phase-shifted $\frac{1}{4}\pi$ with respect to the fundamental, and must force a secondary oscillation on the interior in order that asymptotic matching be satisfied. The radiation from these small vibrations $O((\delta/a)\,u_{\mathrm{m}})$ is equivalent to that from a vibrating sphere of radius $\hat{r} = a+\delta$. The secondary oscillations driven in this way may be taken as irrotational in the interior near field because shear vanishes at the outer edge of the boundary layer and potential flow is fully determined by the instantaneous normal velocities of the boundaries. This outward radiation may be expressed generally as an expansion in solid spherical harmonics (see Morse & Feshbach 1953, p. 1477):

$$\phi^{(2)} = \mathrm{Re}\left\{\frac{1}{4\pi k^{(2)} a}\sum_{n}^{\infty}\sum_{s}^{\infty} \epsilon_s (2n+1)\,\frac{(n-s)!}{(n+s)!}\,\frac{h_n(k^{(2)}ar)}{h_n'(k^{(2)}a)} \right.$$
$$\left. \times P_n^s(\cos\theta)\int_0^{2\pi}\int_0^{\pi} u_{r0}^{(2)}\,P_n^s(\cos\theta)\cos s(\alpha-\alpha_0)\sin\theta\,\mathrm{d}\theta\,\mathrm{d}\alpha_0\right\}. \tag{3.2}$$

Here ϵ_s is Neumann's coefficient, P_n^s is the Legendre function of order s and degree n, h_n is the spherical Hankel function of the first kind and degree n, the prime denotes derivatives with respect to r. The radiation due to the secondary wave will propagate out through the fluid at the speed of sound $\tilde{c}$, so that $\sigma/\sigma_0 = (c/\tilde{c})\,ka \ll 1$. By condition (2.5), ka has been taken as small. The phase speed of the surface gravity waves admissible by (2.6) is negligible with respect to the speed of sound in water. Therefore only the long-wavelength limit to the expansion, where $\sigma/\sigma_0 \to 0$, is of importance here. The lowest-degree solid harmonic that does not vanish over the unit sphere appears at $n = 1$, while solid harmonics of higher degree are negligible to this order. The required integrations reduce the expansion to

$$\frac{\delta}{a}\,\phi^{(2)} = \mathrm{Re}\left\{-\frac{3}{4}\,\frac{\delta}{a}\left(\frac{\sigma}{\sigma_0}\right)^2 h_1\left(\frac{\sigma}{\sigma_0 r}\right)[\cos\theta + \mathrm{i}\tanh\tfrac{1}{2}kh\sin\theta\cos\alpha](1+\mathrm{i})\,\mathrm{e}^{\mathrm{i}t}\right\}. \tag{3.3}$$

The limit to (3.3) many radii out from the sphere decays as $1/r$, becoming negligible, $O((\delta/a)\,(c/\tilde{c})\,ka)$ at the free surface. Consequently, the secondary wave behaves as a non-dispersive acoustic-type disturbance throughout the interior.

Over the near field of the sphere, $r = O(1)$, the secondary wave is given by (3.3) in dimensional form as

$$\frac{\delta}{a}\,\hat{\phi}^{(2)} = \mathrm{Re}\left\{\frac{\delta}{a}\,\tfrac{3}{4}\sqrt{2}\,u_{\mathrm{m}}\,\frac{a^3}{\hat{r}^2}\,[\cos\theta + \mathrm{i}\tanh\tfrac{1}{2}kh\cos\alpha\sin\theta]\,\mathrm{e}^{\mathrm{i}(\sigma t - \frac{1}{4}\pi)}\right\}. \tag{3.4}$$

This is the same dipole as the motion produced by a sphere moving in an otherwise frictionless fluid around a small elliptic orbit whose major and minor axes measured horizontally and vertically are

$$\left.\begin{aligned} \hat{x} &= d_0^{(2)} = \tfrac{3}{2}\sqrt{2}\,\frac{\delta}{a}\,d_0 \\ \text{and} \qquad \hat{z} &= d_0^{(2)} \tanh \tfrac{1}{2}kh. \end{aligned}\right\} \tag{3.5}$$

4. Viscous perturbation of the boundary layer

In this section we determine whether the correction to the interior from the secondary acoustic-wave radiation will further modify the motion in the boundary layer. Collecting the terms from the Navier–Stokes equations together with the corrections to the pressure gradients from the secondary wave yields the following equations of motion to the first viscous perturbation of the Stokes boundary layer:

$$\left(\frac{\partial}{\partial t}-\frac{1}{2}\,\frac{\partial^2}{\partial Y^2}\right) U^{(2)} = \frac{\partial U^{(1)}}{\partial Y} - \left[Y+\frac{1-\mathrm{i}}{2}\right]\frac{\partial u_{\theta_0}^{(1)}}{\partial t}, \tag{4.1}$$

$$\left(\frac{\partial}{\partial t}-\frac{1}{2}\,\frac{\partial^2}{\partial Y^2}\right) W^{(2)} = \frac{\partial W^{(1)}}{\partial Y} - \left[Y+\frac{1-\mathrm{i}}{2}\right]\frac{\partial u_{\alpha_0}^{(1)}}{\partial t}, \tag{4.2}$$

$$\frac{\partial V^{(2)}}{\partial Y} = -\frac{\partial U^{(2)}}{\partial X} - \tanh \tfrac{1}{2}kh\,\frac{\partial W^{(2)}}{\partial Z} - Y\,\frac{\partial V^{(1)}}{\partial Y} - U^{(2)} \cot X - 2V^{(1)}. \tag{4.3}$$

To these the condition of vanishing speed is applied,

$$U^{(2)} = W^{(2)} = V^{(2)} = 0 \quad (Y = 0), \tag{4.4}$$

together with the matching condition, which to this order of approximation requires that

$$\left.\begin{aligned} U^{(2)} &= -Yu_{\theta_0} - \tfrac{1}{2}(1-\mathrm{i})\,u_{\theta_0}^{(1)}, \quad W^{(2)} = -Yu_{\alpha_0} - \tfrac{1}{2}(1-\mathrm{i})\,u_{\alpha_0}^{(1)}, \\ V^{(2)} &= 4Y^2\,\frac{\partial u_{\theta_0}^{(1)}}{\partial \theta} \quad (Y \to \infty). \end{aligned}\right\} \tag{4.5}$$

To (4.1)–(4.3) we assume solutions of the kind

$$U^{(2)} = \beta_{(Y)}\,u_{\theta_0}^{(1)}, \tag{4.6}$$

$$W^{(2)} = \beta_{(Y)}\,u_{\alpha_0}^{(1)}, \tag{4.7}$$

$$V^{(2)} = \gamma_{(Y)}\,\frac{\partial u_{\theta_0}^{(1)}}{\partial \theta}. \tag{4.8}$$

With (4.6)–(4.8), (4.1)–(4.3) reduce to the following forced linear differential equations:

$$\frac{\partial^2 \beta}{\partial Y^2} - 2\mathrm{i}\beta = 1+\mathrm{i}+2\mathrm{i}Y-2(1+\mathrm{i})\,\mathrm{e}^{-(1+\mathrm{i})Y}, \tag{4.9}$$

$$\frac{\partial \gamma}{\partial Y} = 4(\zeta-\beta). \tag{4.10}$$

The solution to (4.9) and (4.10) subject to (4.4) and (4.5) are found after successive integration to be

$$\beta = -Y-\tfrac{1}{2}(1-\mathrm{i})+Y\,\mathrm{e}^{-(1+\mathrm{i})Y}+\tfrac{1}{2}(1-\mathrm{i})\,\mathrm{e}^{-(1+\mathrm{i})Y}, \tag{4.11}$$

$$\gamma = 4Y^2+2(1-\mathrm{i})\,Y\,\mathrm{e}^{-(1+\mathrm{i})Y}. \tag{4.12}$$

As with the $O(1)$ Stokes boundary-layer solution, the tangential oscillations given by the $O(\delta/a)$ solutions limit match with the near field. The boundary-layer solution to oscillations normal to the sphere matches asymptotically through order δ^2/a^2 without further correction to the near field.

5. Advective perturbation of the boundary layer

Having made all lower-order viscous corrections to the boundary-layer profile, we now iterate with that profile in specifying the $O(d_0/D)$ nonlinear curvature terms at this next order of approximation to the Navier–Stokes equation. The $O(d_0/D)$ equations of motion obtained for the boundary layer in this way are forced by products of complex periodic functions. Therefore each admits to separation into time-independent and time-dependent equations. Let the time-independent solutions be denoted by $\langle U^{(3)}\rangle$, $\langle W^{(3)}\rangle$ and $\langle V^{(3)}\rangle$, and the time-dependent parts by $U^{(3)}_{(t)}$, $W^{(3)}_{(t)}$ and $V^{(3)}_{(t)}$. The full $O(d_0/D)$ solutions may be expressed as

$$U^{(3)} = \langle U^{(3)}\rangle + U^{(3)}_{(t)}, \quad W^{(3)} = \langle W^{(3)}\rangle + W^{(3)}_{(t)}, \quad V^{(3)} = \langle V^{(3)}\rangle + V^{(3)}_{(t)}. \tag{5.1}$$

The following equations for the steady tangential $O(d_0/D)$ motion are realized:

$$-\frac{\partial^2}{\partial Y^2}\langle U^{(3)}\rangle = \mathrm{Re}\left\{-\left(1-\zeta'\zeta'^*-2\zeta\frac{\mathrm{d}\zeta'^*}{\mathrm{d}Y}\right)\left[\tfrac{9}{4}\mathrm{i}\tanh\tfrac{1}{2}kh\cos\left(\frac{Z}{\sin X}\right)\right]\right.$$
$$\left.+\left(1-\zeta'\zeta'^*+2\zeta\frac{\mathrm{d}\zeta'^*}{\mathrm{d}Y}\right)\frac{9}{8}\left[1-\tanh^2\tfrac{1}{2}kh\cos^2\left(\frac{Z}{\sin X}\right)\right]\sin 2X\right\}, \tag{5.2}$$

and

$$-\frac{\partial^2}{\partial Y^2}\langle W^{(3)}\rangle = \mathrm{Re}\left\{\left(1-\zeta'\zeta'^*+2\zeta\frac{\mathrm{d}\zeta'^*}{\mathrm{d}Y}\right)\frac{9}{8}\left[\tanh\tfrac{1}{2}kh\sin X\sin\left(\frac{2Z}{\sin X}\right)\right]\right.$$
$$\left.-\left(1-\zeta'\zeta'^*+2\zeta\frac{\mathrm{d}\zeta'^*}{\mathrm{d}Y}\right)\left[\tfrac{9}{4}\cos X\sin\left(\frac{Z}{\sin X}\right)\right]\right\}, \tag{5.3}$$

where asterisks denote complex conjugates. The equations for the unsteady part, which factor out, are

$$\left(\frac{\partial}{\partial t}-\frac{1}{2}\frac{\partial^2}{\partial Y^2}\right)U^{(3)}_{(t)} = \frac{1}{4}\left(1-\zeta'^2+2\zeta\frac{\mathrm{d}\zeta'}{\mathrm{d}Y}\right)(E_1-\mathrm{i}E_2)\,\mathrm{e}^{\mathrm{i}2t}$$
$$+\frac{1}{4}\left(1-\zeta'^*\zeta'^*+2\zeta^*\frac{\mathrm{d}\zeta'^*}{\mathrm{d}Y}\right)(E_1+\mathrm{i}E_2)\,\mathrm{e}^{-\mathrm{i}2t}, \tag{5.4}$$

$$\left(\frac{\partial}{\partial t}-\frac{1}{2}\frac{\partial^2}{\partial Y^2}\right)W^{(3)}_{(t)} = \frac{1}{4}\left(1-\zeta'^2+2\zeta\frac{\mathrm{d}\zeta'}{\mathrm{d}Y}\right)(\mathrm{i}E_3-E_4)\,\mathrm{e}^{\mathrm{i}2t}$$
$$+\frac{1}{4}\left(1-\zeta'^*\zeta'^*+2\zeta^*\frac{\mathrm{d}\zeta'^*}{\mathrm{d}Y}\right)(-\mathrm{i}E_3-E_4)\,\mathrm{e}^{-\mathrm{i}2t}, \tag{5.5}$$

where

$$E_1 = \frac{9}{8}\left[1+\tanh^2\tfrac{1}{2}kh\cos^2\left(\frac{Z}{\sin X}\right)\right]\sin 2X, \quad E_3 = \tfrac{9}{4}\cos X\sin\left(\frac{Z}{\sin X}\right),$$
$$E_2 = \tfrac{9}{4}\tanh\tfrac{1}{2}kh\cos\left(\frac{Z}{\sin X}\right)\cos 2X, \quad E_4 = \tfrac{9}{8}\tanh\tfrac{1}{2}kh\sin X\sin\left(\frac{2Z}{\sin X}\right).$$

The normal $O(d_0/D)$ motions are given by the continuity equation

$$-\frac{\partial V^{(3)}}{\partial Y} = \frac{\partial U^{(3)}}{\partial X} + U^{(3)} \cot X + \tanh \tfrac{1}{2}kh \frac{\partial W^{(3)}}{\partial Z}. \tag{5.6}$$

On these equations the conditions of vanishing surface speed is imposed,

$$U^{(3)} = W^{(3)} = V^{(3)} = 0 \quad (Y = 0), \tag{5.7}$$

plus a matching condition at the outer edge of the boundary layer. We require only that the solution vary slowly across the outer edge of the boundary layer to allow overlap with $O(d_0/D)$ terms in the near field. Therefore we take

$$\frac{\partial U^{(3)}}{\partial Y}, \frac{\partial W^{(3)}}{\partial Y}, \frac{\partial V^{(3)}}{\partial Y} \leqslant O\left(\frac{\delta}{a}\right) \quad (Y \to \infty). \tag{5.8}$$

Solutions to the steady components by successive integrations of (5.2), (5.3) and (5.6) such that the boundary conditions (5.7) and (5.8) are satisfied show that

$$\langle U^{(3)} \rangle = \mathrm{Re}\left\{ \mathrm{i}\tfrac{9}{4}\Pi_2 \tanh \tfrac{1}{2}kh \cos \frac{Z}{\sin X} - \tfrac{9}{8}\Pi_1 \left[1 - \cos^2\left(\frac{Z}{\sin X}\right) \tanh^2 \tfrac{1}{2}kh\right] \sin 2X \right\}, \tag{5.9}$$

$$\langle W^{(3)} \rangle = \mathrm{Re}\left\{ -\tfrac{9}{8}\Pi_1 \tanh \tfrac{1}{2}kh \sin X \sin\left(\frac{2Z}{\sin X}\right) + \tfrac{9}{4}\Pi_1 \cos X \sin\left(\frac{Z}{\sin X}\right) \right\}, \tag{5.10}$$

$$\langle V^{(3)} \rangle = \tfrac{9}{8} \mathrm{Re}\left\{ \Pi_3 3 \left[1 - \tanh^2 \tfrac{1}{2}kh \cos^2\left(\frac{Z}{\sin X}\right)\right] \cos 2X + \Pi_3 \left[3 \tanh^2 \tfrac{1}{2}kh \cos^2\left(\frac{Z}{\sin X}\right) + 1 - 2 \tanh^2 \tfrac{1}{2}kh\right] \right\}, \tag{5.11}$$

where

$$\Pi_1 = (1+\mathrm{i})\, Y\, \mathrm{e}^{-(1-\mathrm{i})Y} + (\tfrac{5}{2}\mathrm{i} - 1)\, \mathrm{e}^{-(1-\mathrm{i})Y} - \tfrac{1}{2}\mathrm{i}\, \mathrm{e}^{-(1+\mathrm{i})Y} - (\tfrac{1}{4} + \tfrac{1}{2}\mathrm{i})\, \mathrm{e}^{-2Y} + \tfrac{5}{4} - \tfrac{3}{2}\mathrm{i},$$

$$\Pi_2 = -(1+\mathrm{i})\, Y\, \mathrm{e}^{-(1-\mathrm{i})Y} + (-\tfrac{3}{2}\mathrm{i} + 1)\, \mathrm{e}^{-(1-\mathrm{i})Y} - \tfrac{1}{2}\mathrm{i}\, \mathrm{e}^{-(1+\mathrm{i})Y} + (\tfrac{1}{2}\mathrm{i} - \tfrac{1}{4})\, \mathrm{e}^{-2Y} - \tfrac{3}{4} + \tfrac{3}{2}\mathrm{i},$$

$$\Pi_3 = -\mathrm{i}\, Y\, \mathrm{e}^{-(1-\mathrm{i})Y} + (\tfrac{5}{2} - \mathrm{i})\, \mathrm{e}^{-(1-\mathrm{i})Y} + (\tfrac{1}{8} + \tfrac{1}{4}\mathrm{i})\, \mathrm{e}^{-2Y} + \tfrac{5}{4}Y - \tfrac{3}{2}\mathrm{i}Y + \tfrac{3}{4}\mathrm{i} - \tfrac{21}{8}.$$

The steady tangential component in (5.9), which varies as Π_2 across the boundary layer, was excited by the progressive-type θ-component of the fundamental oscillation in (2.10). It has a profile similar to the steady streaming resulting from a progressive disturbance in two dimensions (Longuet-Higgins 1953). Those components of (5.9) and (5.10) that vary as Π_1 were excited by the standing part of the fundamental oscillation in (2.10) and (2.11). They resemble the steady-streaming profiles found in two-dimensional boundary layers driven by standing oscillations considered in Schlichting (1932), Eckart (1948) and Longuet-Higgins (1953). The normal streaming component is found to grow linearly in Y, but remains small, $O(d_0\,\delta/D^2)$, in the neighbourhood of $Y \to O(1)$.

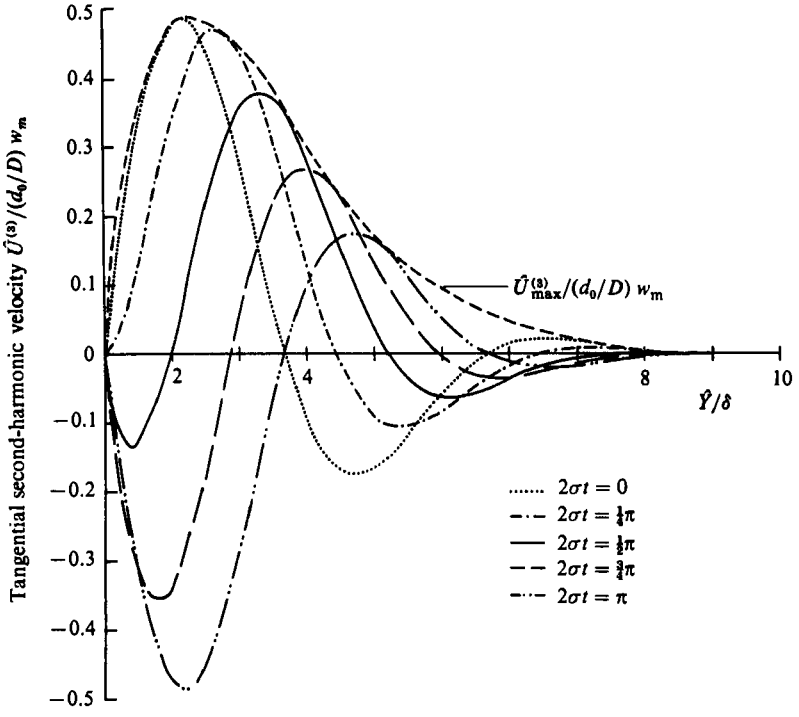

FIGURE 2. Successive profiles of the tangential second-harmonic oscillation at $\frac{1}{8}$-cycle intervals across the boundary layer. These profiles were evaluated at the locus $\theta = \frac{1}{2}\pi$, $\alpha = 0$.

For the unsteady $O(d_0/D)$ boundary-layer motions from (5.4)–(5.6) we assume solutions that are separable as

$$U^{(3)}_{(\ell)} = \xi'(Y)\,(E_1 - \mathrm{i}E_2)\,\mathrm{e}^{\mathrm{i}2t} + \xi'^*(Y)\,(E_1 + \mathrm{i}E_2)\,\mathrm{e}^{-\mathrm{i}2t}, \tag{5.12}$$

$$W^{(3)}_{(\ell)} = \xi'(Y)\,(\mathrm{i}E_3 - E_4)\,\mathrm{e}^{\mathrm{i}2t} + \xi'^*(Y)\,(-\mathrm{i}E_3 - E_4)\,\mathrm{e}^{-\mathrm{i}2t}, \tag{5.13}$$

$$-\frac{\partial V^{(3)}_{(\ell)}}{\partial Y} = \xi'(Y)\,(E_5 + \mathrm{i}E_6)\,\mathrm{e}^{\mathrm{i}2t} + \xi'^*(Y)\,(E_5 - \mathrm{i}E_6)\,\mathrm{e}^{-\mathrm{i}2t}, \tag{5.14}$$

where

$$E_5 = \frac{9}{4}\left\{3\left[1 + \tanh^2 \tfrac{1}{2}kh \cos^2\left(\frac{Z}{\sin X}\right)\right]\cos^2 X - 3\tanh^2 \tfrac{1}{2}kh \cos^2\left(\frac{Z}{\sin X}\right) + \tanh^2 \tfrac{1}{2}kh - 1\right\},$$

$$E_6 = \tfrac{27}{4}\tanh \tfrac{1}{2}kh \cos\left(\frac{Z}{\sin X}\right)\sin 2X.$$

These solutions reduce (5.4) and (5.5) to the following second-order linear differential equation:

$$2\mathrm{i}\xi' - \frac{1}{2}\frac{\mathrm{d}^2\xi'}{\mathrm{d}Y^2} = \tfrac{1}{4} - \tfrac{1}{4}\xi'^2 + \frac{\xi}{2}\frac{\mathrm{d}\xi'}{\mathrm{d}Y}. \tag{5.15}$$

Integrating (5.15) such that the boundary conditions (5.7) and (5.8) are met by an appropriate choice of integration constants yields

$$\xi_{(Y)} = \frac{9(1+\mathrm{i})}{16\sqrt{2}}\,\mathrm{e}^{-(1+\mathrm{i})\sqrt{2}\,Y} - \tfrac{1}{4}(1+\mathrm{i})\,\mathrm{e}^{-(1+\mathrm{i})Y} - \frac{1+\mathrm{i}}{32}\,\mathrm{e}^{-2(1+\mathrm{i})Y} + \tfrac{1}{2}\mathrm{i}Y\,\mathrm{e}^{-(1+\mathrm{i})Y} + (1+\mathrm{i})\left(\tfrac{9}{32} - \tfrac{9}{16\sqrt{2}}\right). \tag{5.16}$$

The second-harmonic boundary-layer profile on a sphere is plotted in figure 2. It contains an additional viscous wave $e^{-2(1+i)\tilde{Y}/\delta}$, absent from the two-dimensional solution of Schlichting (1932). The envelope of tangential second-harmonic oscillations is seen to damp out at the outer edge of the boundary layer. The normal second-harmonic vibrations do not, but rather take on a normally invariant modal pattern $O((d_0\delta/D^2)u_m)$.

6. Second-harmonic oscillation

The normal second-harmonic vibrations of the outer edge of the boundary layer from (5.14) and (5.16) are smaller than the phase-shifted secondary vibrations by a factor $O(d_0/D)$ and will likewise radiate as an irrotational oscillation into the interior. The second-harmonic radiation will be found by the expansion in solid spherical harmonics given in (3.2) for two distinct normal velocity distributions. One of these will be the deep-water form of (5.14), where $\tanh\frac{1}{2}kh\to1$, while the other will be the shallow form, where $\tanh\frac{1}{2}kh\to0$. Either expansion for the second-harmonic radiation will proceed in the long-wavelength limit $2\sigma/\sigma_0\to0$, according to the assumption made in (2.5) and (2.6). The first non-zero solid harmonic does not appear until degree $n=2$. Solid harmonics of higher degree present only higher-order terms in $2\sigma/\sigma_0$. Integrating and summing over three orders, $s=0,1,2$, in the second-degree solid harmonic yields

$$\phi^{(3)} = \mathrm{Re}\left\{\tfrac{27}{2}(\tfrac{1}{2}-\tfrac{1}{\sqrt{2}})\left(\frac{\sigma}{\sigma_0}\right)^3 h_2\left(\frac{2\sigma}{\sigma_0 r}\right)\right.$$
$$\left.\times[(1-i)\sin^2\theta\cos^2\alpha-(1-i)\cos^2\theta-(1+i)\cos\alpha\sin2\theta]\,e^{i2t}\right\}\quad(\tanh\tfrac{1}{2}kh\to1),\tag{6.1}$$

$$\phi^{(3)} = \mathrm{Re}\left\{-\tfrac{72}{16}(\tfrac{1}{2}-\tfrac{1}{\sqrt{2}})\left(\frac{\sigma}{\sigma_0}\right)^3 h_2\left(\frac{2\sigma}{\sigma_0 r}\right)[\cos2\theta+\cos^2\theta](1-i)\,e^{i2t}\right\}\quad(\tanh\tfrac{1}{2}kh\to0),\tag{6.2}$$

where
$$h_2\left(\frac{2\sigma}{\sigma_0 r}\right) = -\frac{4i(\sigma/\sigma_0)^2r^2+6\sigma/\sigma_0 r+3i}{8(\sigma/\sigma_0)^3r^3}\,e^{i2\sigma/\sigma_0 r}.$$

Near the free surface, as $r\to\infty$, both second-harmonic waves (6.1) and (6.2) are small, $O((d_0\delta/D^2)(c^2/\tilde{c}^2)k^2a^2)$, and decay as $1/r$. Therefore the second harmonic radiates through the interior as an acoustic wave to the order of approximation taken in (2.5) and (2.6).

Over the near field of the sphere both second-harmonic waves decay as $1/r^3$. These waves represent simple source distributions. The deep-water expression (6.1) represents a second-harmonic disturbance progressing around the transverse horizontal axis of the sphere as $e^{i(2\alpha'+2\sigma t+\frac{1}{4}\pi)}$ and decaying transversely as $\sin^2\theta'$. The shallow-water second harmonic (6.2) has axisymmetry about the axis of wave advance and represents a standing disturbance with antinodes at both the up- and downwave poles, $\theta=0,\pi$. Both second-harmonic oscillations lead the fundamental oscillation in the near field by $\frac{1}{4}\pi$.

7. Steady streaming in the near field

The tangential steady streaming generated by the Reynolds stresses across the boundary layer in §5 will now force an $O((d_0/D)u_m)$ correction on the interior through the matching condition. For a deep-water incident wave, the matching boundary

condition is reduced in dependence to a single polar variable when transformed to the (x', y', z') rotated system, giving

$$\lim_{Y\to\infty} \langle \boldsymbol{U}^{(3)} \rangle \equiv \lim_{r\to 1} \langle \boldsymbol{u} \rangle \equiv \boldsymbol{n}_{\theta'} \langle u_{\theta' 0} \rangle + \boldsymbol{n}_{\alpha'} \langle u_{\alpha' 0} \rangle$$
$$= -\boldsymbol{n}_{\alpha'} \tfrac{27}{8} \sin\theta' + \boldsymbol{n}_{\theta'} \tfrac{45}{32} \sin 2\theta' \quad (\tanh \tfrac{1}{2}kh \to 1). \tag{7.1}$$

Similarly, the matching condition under a plane shallow-water incident wave simplifies in the primary (x, y, z) system to

$$\lim_{Y\to\infty} \langle \boldsymbol{U}^{(3)} \rangle = \lim_{r\to 1} \langle \boldsymbol{u} \rangle = -\boldsymbol{n}_{\theta} \tfrac{45}{32} \sin 2\theta \quad (\tanh \tfrac{1}{2}kh \to 0), \tag{7.2}$$

where $(\boldsymbol{n}_r, \boldsymbol{n}_\theta, \boldsymbol{n}_\alpha)$ and $(\boldsymbol{n}_r, \boldsymbol{n}_{\theta'}, \boldsymbol{n}_{\alpha'})$ are polar unit vectors in the primary and rotated systems and where $\boldsymbol{n}_r \langle \hat{u}_{r_0} \rangle = O(d_0 \delta / D^2)$.

The deep-water case (7.1) has two orthogonal streaming velocity components. The $\langle u_{\alpha' 0} \rangle$ component is concentric about the transverse axis and is the unidirectional steady streaming due to the progressive part of the fundamental oscillation (2.10). It will be referred to as the 'circulation streaming'. The circulation-streaming term in (7.1) is identical with the relative surface speeds if the spherical surface at the outer edge of the boundary layer were in solid-body rotation about the transverse axis oy or ox' with an angular rotation rate Ω_0 equal to

$$\hat{\Omega}_0 = \frac{27}{8} \frac{d_0 u_m}{D(a+\delta)} \tanh \tfrac{1}{2}kh \sim \frac{27}{4} \frac{d_0}{D^2} u_m \tanh \tfrac{1}{2}kh. \tag{7.3}$$

The $\langle u_{\theta' 0} \rangle$ component in (7.1) is identical in form with the steady streaming in the plane shallow-water-wave case (7.2), with each being axisymmetric about the transverse axis oy and the axis of wave advance ox respectively. These streaming components are referred to as 'acoustic streaming' resulting from the standing part of the fundamental oscillation (2.10) and (2.11).

The properties of concentricity and axisymmetry in these two limiting forms of the matching boundary condition, (7.1) and (7.2), render description of the resulting Eulerian streaming field in terms of the orthogonal functions ψ and Γ, where

$$\left.\begin{aligned} \langle u_{\theta'} \rangle &= \frac{1}{r \sin\theta'} \frac{\partial \psi}{\partial r}, \\ \langle u_r \rangle &= \frac{1}{r^2 \sin\theta'} \frac{\partial \psi}{\partial \theta'}, \\ \langle u_{\alpha'} \rangle &= \frac{\Gamma}{r \sin\theta'} \end{aligned}\right\} \quad (\tanh \tfrac{1}{2}kh \to 1), \tag{7.4}$$

and
$$\langle u_\theta \rangle = -\frac{1}{r \sin\theta} \frac{\partial \psi}{\partial r}, \quad \langle u_r \rangle = \frac{1}{r^2 \sin\theta} \frac{\partial \psi}{\partial \theta} \quad (\tanh \tfrac{1}{2}kh \to 0). \tag{7.5}$$

ψ defines the acoustic-streaming field and Γ defines the circulation-streaming field. Solutions for the intermediate case, $0 < w_m/u_m < 1$, are frustrated by the non-existence of a stream function, as a consequence of the three-dimensionality of the boundary-layer-driven streaming in this regime.

With this change of variables, the equations for steady streaming in the near field by diffusive vorticity transport, $R^{(2)} \to 0$, are given as

$$\mathrm{L}'(\mathrm{L}'\psi^{(3)}) = 0, \tag{7.6}$$

$$\mathrm{L}'\Gamma^{(3)} = 0 \quad (\tanh \tfrac{1}{2}kh \to 1), \tag{7.7}$$

$$\left.\begin{aligned} &\frac{1}{r}\frac{\partial \psi^{(3)}}{\partial r} = -\tfrac{45}{32}\sin\theta' \sin 2\theta', \\ &\frac{\psi^{(3)}}{r^2} = 0, \quad \frac{\Gamma^{(3)}}{r} = -\tfrac{27}{8}\sin^2\theta' \end{aligned}\right\} \quad (r \to 1), \tag{7.8}$$

$$\frac{\psi^{(3)}}{r^2} = \frac{1}{r}\frac{\partial \psi^{(3)}}{\partial r} = 0, \quad \frac{\Gamma^{(3)}}{r} = 0 \quad (r \to \infty), \tag{7.9}$$

and

$$\mathrm{L}(\mathrm{L}\psi^{(3)}) = 0 \quad (\tanh \tfrac{1}{2}kh \to 0), \tag{7.10}$$

$$\frac{1}{r}\frac{\partial \psi^{(3)}}{\partial r} = \tfrac{45}{32}\sin\theta \sin 2\theta, \quad \frac{\psi^{(3)}}{r^2} = 0 \quad (r \to 1), \tag{7.11}$$

$$\frac{\psi^{(3)}}{r^2} = \frac{1}{r}\frac{\partial \psi^{(3)}}{\partial r} = 0 \quad (r \to \infty), \tag{7.12}$$

where L and L′ are the ∇^2 operators in spherical polar coordinates (r, θ, α) and (r, θ', α') respectively, with $\partial/\partial\alpha = \partial/\partial\alpha' = 0$.

Proceeding now with solutions to the diffusive streaming under a deep-water wave, the matching boundary condition (7.8) suggests separating variables by seeking solutions to (7.6) of the form

$$\psi = AM(r)\sin\theta' \sin 2\theta', \tag{7.13}$$

where A is a constant to be determined. This reduces (7.6) to the following fourth-order equidimensional differential equation:

$$r^4\frac{\mathrm{d}^4M}{\mathrm{d}r^4} - 12r^2\frac{\mathrm{d}^2M}{\mathrm{d}r^2} + 24r\frac{\mathrm{d}M}{\mathrm{d}r} = 0. \tag{7.14}$$

A power solution to (7.14) subject to (7.8) and (7.9) proceeds readily according to methods outlined in Hildebrand (1963). The resulting solution for the acoustic-streaming field under a deep-water wave is

$$\psi^{(3)} = -\frac{45}{64}\left(1 - \frac{1}{r^2}\right)\sin\theta' \sin 2\theta' \quad (\tanh \tfrac{1}{2}kh \to 1). \tag{7.15}$$

Solutions to (7.10) subject to (7.11) and (7.12) proceed identically with those for a deep-water wave. Thus the field of steady streaming under a plane shallow-water wave is given by

$$\psi^{(3)} = \frac{45}{64}\left(1 - \frac{1}{r^2}\right)\sin\theta \sin 2\theta \quad (\tanh \tfrac{1}{2}kh \to 0). \tag{7.16}$$

The complementary function $\Omega^{(3)}$ will render further simplification for diffusive solutions to the circulation-streaming field from (7.7), where

$$\int \Omega^{(3)} r\,\mathrm{d}r = \frac{\Gamma^{(3)}}{\sin^2\theta'}. \tag{7.17}$$

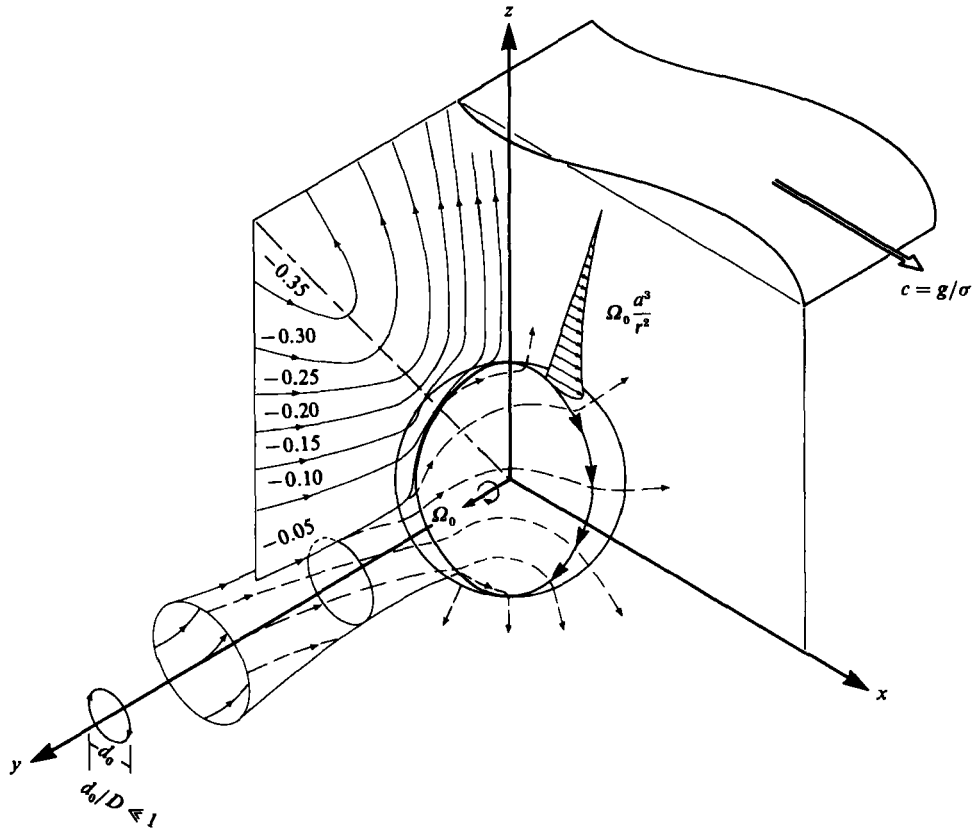

FIGURE 3. Axonometric representation of the Eulerian streaming field near a sphere due to a diffusive steady-state vorticity distribution in the interior of a deep-water surface wave. The acoustic streaming is shown in a vertical plane transverse to the surface wave. The tangential velocity due to the circulation streaming is profiled radially in a vertical plane along the direction of wave advance. The sum of the two streaming fields is portrayed by the swirling streamtube.

Here $\Omega^{(3)}$ is the angular-rotation rate of a spherical shell of fluid of radius r, about the transverse axis ox'. Substitution of (7.17) in (7.7) reduces the equation of motion to that for a slowly rotating sphere in an infinite volume of still fluid as given in Lamb (1932, Art. 334). The solution when the rotation rate is specified according to (7.3) is

$$\Omega = \frac{\Omega_0}{r^3} \quad \text{or} \quad \Gamma^{(3)} = -\frac{27}{8}\frac{\sin^2\theta'}{r}. \tag{7.18}$$

Thus when $R^{(2)} \to 0$ the circulation–streaming vorticity is distributed through the interior on concentric spherical shells. These rotate about the transverse axis, with the rotation rate decaying into the interior as $1/r^3$ from a value of Ω_0 at the top of the boundary layer.

The steady tangential components at the $O(d_0/D)$ limit match according to (7.1) and (7.2). The normal steady components match asymptotically, leaving a residual error $O(d_0\delta^2/D^3)u_m$).

Axonometric representations of the complete three-dimensional diffusive Eulerian streaming are given in figure 3 under a deep-water incident wave. The diffusive

acoustic streaming shown in the transverse meridional plane under a deep-water wave is the same streamline pattern as that found by Bickley (1936) for the transverse streaming on a rotating sphere. The streaming is reversed in meridional planes through the axis of wave advance under a plane shallow-water wave. The shallow-water solution (7.16) is equivalent to one for a sphere in sound waves found by Andrews & McIntyre (1978), using a different method.

8. Advective perturbation of the diffusive interior

This section continues under the hypothesis that the Reynolds number remains small, $R^{(2)} \ll 1$, without being vanishingly small as assumed in §7. The advective terms omitted from the right-hand side of the vorticity-transport equations (7.6), (7.7) or (7.10) are $O(R^{(2)})$. Therefore a perturbation of the steady diffusive solutions might be assumed of the form

$$\psi = \frac{d_0}{D}\psi^{(3)} + \frac{d_0^3}{2D\delta^2}\psi^{(4)}, \quad \Gamma = \frac{d_0}{D}\Gamma^{(3)} + \frac{d_0^3}{2D\delta^2}\Gamma^{(4)}. \tag{8.1}$$

The diffusive solutions $\psi^{(3)}$ and $\Gamma^{(3)}$ are sufficiently well behaved that such a low-Reynolds-number perturbation will not become singular in the far field, as found in low-Reynolds-number steady flows – Stokes and Whitehead's paradox. A typical advective term by iteration with the diffusive solution will be $O(R^{(2)}/r^5)$ as $r \to \infty$. A typical viscous term from a cross-product on the left-hand side of (7.6) or (7.10) becomes $O(1/r^4)$ as $r \to \infty$. Hence the low-Reynolds-number hypothesis remains valid in the far field since

$$\frac{\text{advective terms}}{\text{viscous terms}} = O\left(\frac{R^{(2)}}{r}\right) \quad (r \to \infty).$$

The vorticity-transport equations for the advective perturbation of the interior streaming may then be written (see Goldstein 1938, pp. 114–115),

$$\mathrm{L}'(\mathrm{L}'\psi^{(4)}) = \frac{1}{r^2 \sin\theta'}\left\{\frac{\partial\psi^{(3)}}{\partial\theta'}\frac{\partial}{\partial r} - \frac{\partial\psi^{(3)}}{\partial r}\frac{\partial}{\partial\theta'} + 2\frac{\partial\psi^{(3)}}{\partial r}\cot\theta' - \frac{2}{r}\frac{\partial\psi^{(3)}}{\partial\theta'}\right\}\mathrm{L}'\psi^{(3)}$$
$$+ \frac{1}{r^2\sin\theta'}\left(2\Gamma^{(3)}\frac{\partial\Gamma^{(3)}}{\partial r}\cot\theta' - \frac{2}{r}\Gamma^{(3)}\frac{\partial\Gamma^{(3)}}{\partial\theta'}\right), \tag{8.2}$$

$$\mathrm{L}'\Gamma^{(4)} = \frac{1}{r^2\sin\theta'}\left(\frac{\partial\psi^{(3)}}{\partial\theta'}\frac{\partial\Gamma^{(3)}}{\partial r} - \frac{\partial\psi^{(3)}}{\partial r}\frac{\partial\Gamma^{(3)}}{\partial\theta'}\right) \quad (\tanh\tfrac{1}{2}kh \to 1), \tag{8.3}$$

$$\mathrm{L}(\mathrm{L}\psi^{(4)}) = \frac{1}{r^2\sin\theta}\left\{\frac{\partial\psi^{(3)}}{\partial\theta}\frac{\partial}{\partial r} - \frac{\partial\psi^{(3)}}{\partial r}\frac{\partial}{\partial\theta}\right.$$
$$\left. + 2\frac{\partial\psi^{(3)}}{\partial r}\cot\theta - \frac{2}{r}\frac{\partial\psi^{(3)}}{\partial\theta}\right\}\mathrm{L}\psi^{(3)} \quad (\tanh\tfrac{1}{2}kh \to 0), \tag{8.4}$$

where

$$\frac{1}{r}\frac{\partial\psi^{(4)}}{\partial r} = \frac{\psi^{(4)}}{r^2} = 0 \quad (r \to 1), \tag{8.5}$$

$$\Gamma^{(4)}/r = 0 \quad (r \to 1), \tag{8.6}$$

$$\frac{1}{r}\frac{\partial\psi^{(4)}}{\partial r} = \frac{\psi^{(4)}}{r^2} = 0 \quad (r \to \infty), \tag{8.7}$$

$$\Gamma^{(4)}/r = 0 \quad (r \to \infty). \tag{8.8}$$

Consider first solutions to the advective deep-water acoustic streaming field $\psi^{(4)}$. Inserting the diffusive solutions $\psi^{(3)}$ and $\Gamma^{(3)}$ into the right-hand side of (8.2) renders a separation of variables by seeking a solution of the form

$$\psi^{(4)} = N'(r)\cos\theta' \sin^2 2\theta' + \mathcal{O}'(r)\sin\theta \sin 2\theta', \tag{8.9}$$

where N' and $\mathcal{O}'$ are functions of r to be determined. Equation (8.9) will then separate (8.2) into two simultaneous fourth-order inhomogeneous ordinary differential equations:

$$r^4\frac{\mathrm{d}^4N'}{\mathrm{d}r^4} - 40r^2\frac{\mathrm{d}^2N'}{\mathrm{d}r^2} + 80r\frac{\mathrm{d}N'}{\mathrm{d}r} + 280N' = \frac{6075}{512}\left(\frac{3}{r} - \frac{5}{2r^3}\right), \tag{8.10}$$

$$r^4\frac{\mathrm{d}^4\mathcal{O}'}{\mathrm{d}r^4} - 12r^2\frac{\mathrm{d}^2\mathcal{O}'}{\mathrm{d}r^2} + 24r\frac{\mathrm{d}\mathcal{O}'}{\mathrm{d}r} = \frac{6075}{512}\left(-\frac{366}{75r} + \frac{1}{r^3}\right) - 24r^2\frac{\mathrm{d}^2N'}{\mathrm{d}r^2} + 48r\frac{\mathrm{d}N'}{\mathrm{d}r}. \tag{8.11}$$

Following procedures detailed in Hildebrand (1963), the solutions to (8.10) and (8.11) subject to (8.5) and (8.7) are found to be

$$N'_{(r)} = -\frac{0.061798}{r^4} + \frac{0.370788}{r^3} - \frac{0.556182}{r^2} + \frac{0.247192}{r}, \tag{8.12}$$

$$\mathcal{O}'_{(r)} = \frac{0.052928}{r^4} - \frac{0.411874}{r^3} + \frac{0.04729}{r^2} + \frac{0.92930}{r} - 0.61762. \tag{8.13}$$

Turning attention now to the advective-circulation streaming field, (8.3) admits to a separation of variables by assuming a solution of the form:

$$\Gamma^{(4)} = G(r)\sin^2 2\theta' + K(r)\sin^2\theta'. \tag{8.14}$$

By (8.14), (8.3) is decomposed into the following simultaneous second-order ordinary differential equations:

$$r^2\frac{\mathrm{d}^2G}{\mathrm{d}r^2} - 12G = \frac{1}{r^2}\,\frac{3645}{1024} + \frac{1}{r^4}\,\frac{1215}{1024}, \tag{8.15}$$

$$r^2\frac{\mathrm{d}^2K}{\mathrm{d}r^2} - 2K = -\frac{1}{r^2}\,\frac{1215}{256} + \frac{1}{r^4}\,\frac{1215}{256} - 8G. \tag{8.16}$$

Similarly the solutions to (8.15) and (8.16) subject to (8.6) and (8.8) are

$$G = \frac{1}{r^4}\,\frac{1215}{8192} + \frac{1}{r^3}\,\frac{10935}{24576} - \frac{1}{r^2}\,\frac{3645}{6144}, \tag{8.17}$$

$$K(r) = \frac{1}{r^4}\,\frac{3645}{18432} - \frac{1}{r^3}\,\frac{3645}{10240} + \frac{1}{r}\,\frac{729}{4608}. \tag{8.18}$$

This completes the solutions to the low-Reynolds-number perturbation of the interior field of steady streaming when $\tanh\frac{1}{2}kh = 1$. For the advective-streaming correction under a plane shallow-water wave, (8.4) is written with the diffusive solutions for $\psi^{(3)}$ from (7.17). Again a separation of variables may be achieved by assuming a solution of the form,

$$\psi^{(4)} = N(r)\cos\theta \sin^2 2\theta + \mathcal{O}(r)\sin\theta \sin 2\theta. \tag{8.19}$$

Substituting (8.19) into (8.4) will result in a pair of simultaneous fourth-order inhomogeneous ordinary differential equations. The equation for N is identical with (8.10) and subject to the same boundary conditions. Therefore

$$N = N', \tag{8.20}$$

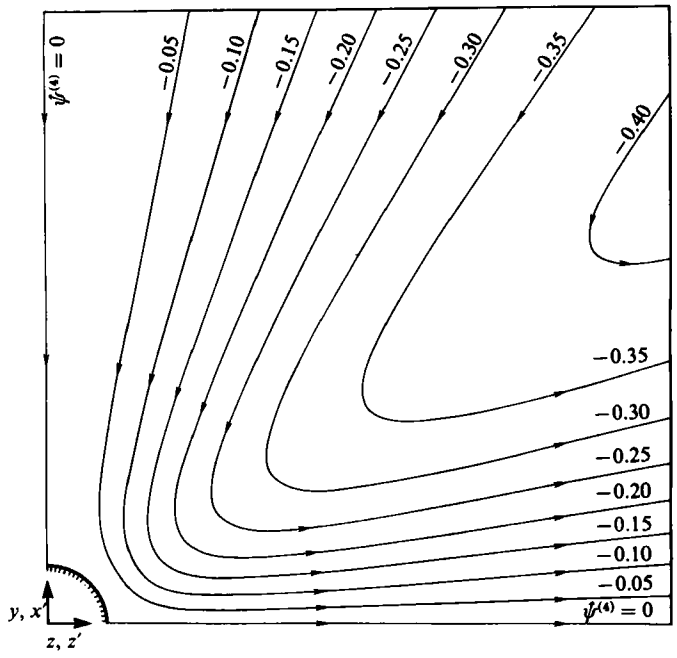

FIGURE 4. Streamlines due to the advective acoustic streaming $\psi^{(4)}$ under a deep-water incident wave. The acoustic streaming is shown in a vertical meridional plane that is transverse to the surface wave about oy or ox'.

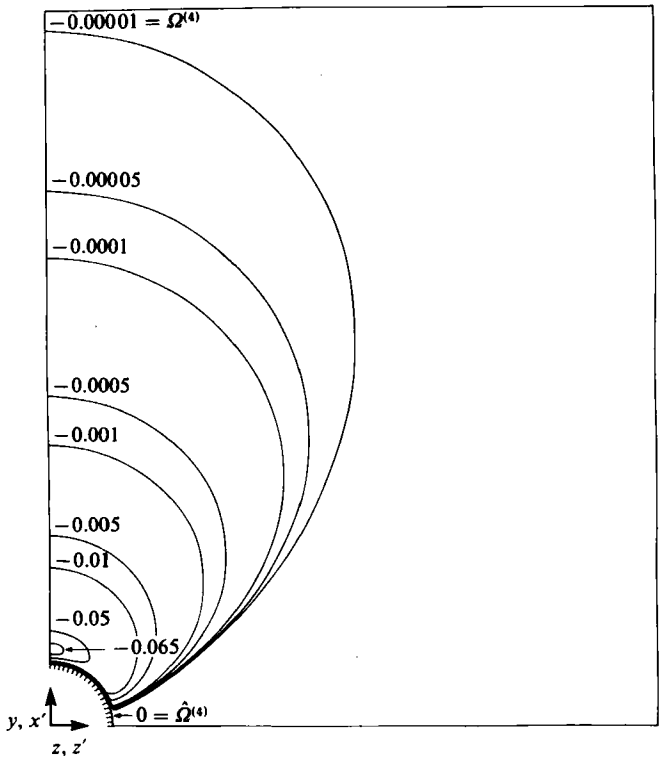

FIGURE 5. Lines of constant vorticity due to the advective circulation streaming $\Omega^{(4)}$. The curves are shown in a vertical plane through the transverse axis oy or ox'.

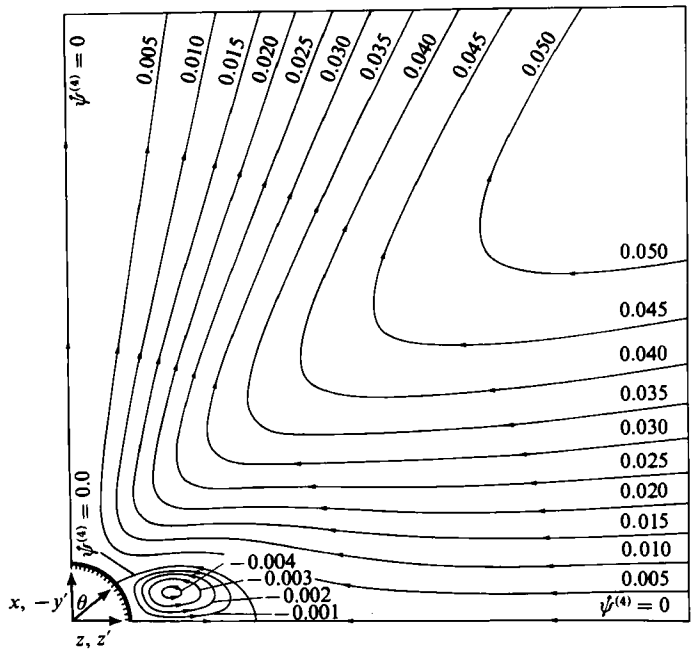

FIGURE 6. Streamlines due to the advective acoustic streaming $\psi^{(4)}$ under a plane linearized shallow-water incident wave. The acoustic streaming is shown in a vertical meridional plane that lies along the axis of wave advance ox.

where the solution to N' is given by (8.12). The remaining equation separated from (8.4) is

$$r^4\frac{\mathrm{d}^4\mathscr{O}}{\mathrm{d}r^4}-12r^2\frac{\mathrm{d}^2\mathscr{O}}{\mathrm{d}r^2}+24r\frac{\mathrm{d}\mathscr{O}}{\mathrm{d}r}=\frac{6075}{512}\left(-\frac{2}{r}+\frac{1}{r^3}\right)-24r^2\frac{\mathrm{d}^2N}{\mathrm{d}r^2}+48r\frac{\mathrm{d}N}{\mathrm{d}r}+240N. \quad (8.21)$$

Inserting (8.12) in (8.21) and enforcing the boundary conditions (8.5) and (8.7) yields the following solution:

$$\mathscr{O}(r)=\frac{0.052928}{r^4}-\frac{0.411874}{r^3}+\frac{0.75917}{r^2}-\frac{0.49446}{r}+0.094236. \quad (8.22)$$

Our solutions fully complete, we can draw the streamline pattern in figure 4 for the deep-water advective acoustic streaming from (8.9). It is found that the advective-transport process in the interior has shifted the partition between the inflow and outflow away from the value $\theta' = 55°$ characteristic of the diffusive solution in figure 3. Instead, the inflow region has enlarged, while outflow has been confined to a narrowing radial jet about the vertical equator. These features spawned here at low Reynolds numbers resemble the centrifugal pumping due to a rotating sphere at high Reynolds numbers, $\Omega_0 a^2/\nu \gg 1$, treated by Howarth (1951). This Reynolds number is $O(R^{(2)})$ if Ω_0 is taken as in (7.3).

Advective distortion of the circulation streaming under a deep-water wave can be seen in figure 5 on the surfaces of constant vorticity $\Omega^{(4)}$ deduced from (8.14). The solution is equivalent to concentric oblate caps rotating about the transverse axis opposed to the diffusive-circulation rotation. Thus the advective correction $\Gamma^{(4)}$ will diminish the total circulation $\Gamma^{(3)}+R^{(2)}\Gamma^{(4)}$ in the neighbourhood of the transverse poles analogously to the loss of circulation near the tips of a three-dimensional wing.

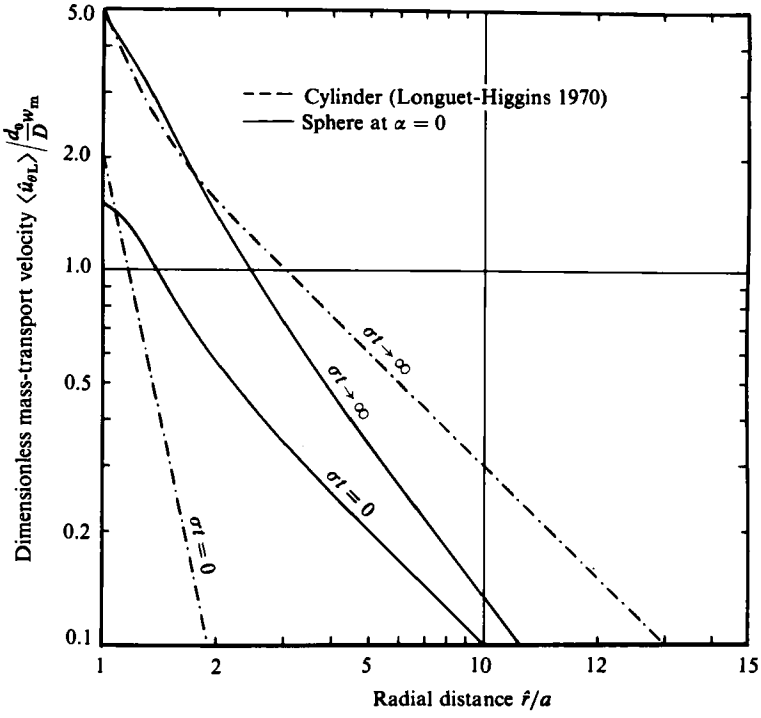

FIGURE 7. Radial profiles of the initial and steady-state θ-component of the mass-transport velocity $\langle u_{\theta L} \rangle$ on a horizontal cylinder and sphere under a deep-water surface wave. The solid curves are evaluated on the vertical equator of a sphere, $\alpha = 0$.

The advective correction to the diffusive acoustic streaming under a plane shallow-water wave, (8.19), has a surprising new feature pictured in figure 6. A pair of stationary steady ring vortices are inferred from this meridional-section view. These steady eddies are paired around the transverse vertical equator where the vorticity and the gradients of vorticity in the boundary layer are a maximum. They persist here around the updrift belt of the sphere in consequence of vorticity advection remaining weak with respect to vorticity diffusion, $R^{(2)} \ll 1$.

9. Near-field Stokes drift and mass transport

The Stokes drift $\langle u_s \rangle$ and the diffusive Eulerian streaming $\langle u^{(3)} \rangle$ are of the same order, $O(u_m d_0/D)$. Their combined effect gives the steady-state mass-transport velocity $\langle u_L \rangle$, where

$$\langle \hat{\boldsymbol{u}}_L \rangle = \langle \hat{\boldsymbol{u}}_s \rangle + \langle \hat{\boldsymbol{u}}^{(3)} \rangle, \quad \langle \hat{\boldsymbol{u}}_s \rangle = \left\langle \int \hat{\boldsymbol{u}}^{(1)} \, \mathrm{d}\hat{\boldsymbol{t}} \cdot \hat{\nabla} \hat{\boldsymbol{u}}^{(1)} \right\rangle. \tag{9.1}$$

The Stokes-drift part of mass transport is irrotational and is established with the initiation of the fundamental oscillation at $t = 0$. With the fundamental oscillation in the near field of the sphere specified by (2.9) the Stokes drift becomes

$$\langle \hat{\boldsymbol{u}}_s \rangle = \boldsymbol{n}_\theta \frac{d_0}{D} u_m \left[-\frac{3}{4} \left(\frac{a^4}{\hat{r}^4} - \frac{a^7}{\hat{r}^7} \right) - \left(\frac{a}{\hat{r}} + \frac{1}{2} \frac{a^4}{\hat{r}^4} \right) \right] \tanh \tfrac{1}{2} kh \cos \alpha$$
$$+ \boldsymbol{n}_\alpha \frac{d_0}{D} u_m \left[\frac{3}{4} \left(\frac{a^4}{\hat{r}^4} - \frac{a^7}{\hat{r}^7} \right) \right] \tanh \tfrac{1}{2} kh \sin \alpha \cos \theta. \tag{9.2}$$

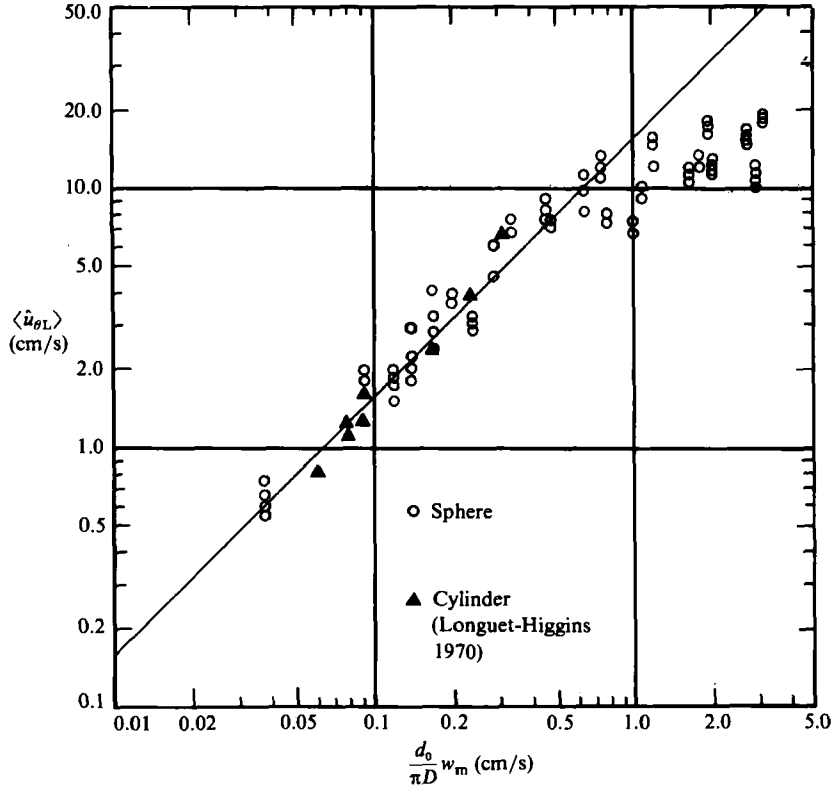

FIGURE 8. The mass-transport velocity $\langle \hat{u}_{\theta L} \rangle$ along the circumference, $\alpha = 0$, of a sphere under laboratory waves. The solid line is the theoretical average mass-transport velocity around the vertical equator on the lower hemisphere of a sphere according to (9.3).

The Stokes drift in (9.2) is everywhere tangential to the spherical surface, decaying in the interior of the wave as $1/r$ for $r \to \infty$.

Substituting (9.2) and (7.4) into (9.1) can give the initial and final θ-component of the mass-transport velocities around the vertical equator of a sphere, $\alpha = 0$, as a function of the radial excursion under a deep-water wave, $w_m/u_m = 1$, shown in figure 7. For comparison, similar results for a cylinder derived from Longuet-Higgins (1970) are included. Initially, at $t = 0$, only Stokes drift contributes to mass transport. All the vorticity is in the boundary layer, so that the diffusive Eulerian streaming has not yet developed in the interior. With a final steady-state vorticity distribution as $t \to \infty$, the drift and streaming fields combine linearly under the hypothesis of non-interaction between the irrotational and rotational motions.

Figure 8 gives laboratory results for timing the drift of the leading edge of a dye streak that was introduced into the boundary layer through a 0.1 cm internally mounted injection port located on the vertical equator at $\alpha = \theta = 0$. The observations were made in the 2.5 m wide wind/wave channel in the Scripps Institution Hydraulics Laboratory using a polished 20 cm diameter sphere fixed by a 0.5 cm diameter strut at mid-depth in 154 cm of water. Discrete frequency waves of 0.2, 0.3, 0.4, 0.5, 0.6 and 0.75 Hz were generated independently with heights of 5–20 cm. This range of heights and frequencies spanned the regime of unseparated flow up to and including

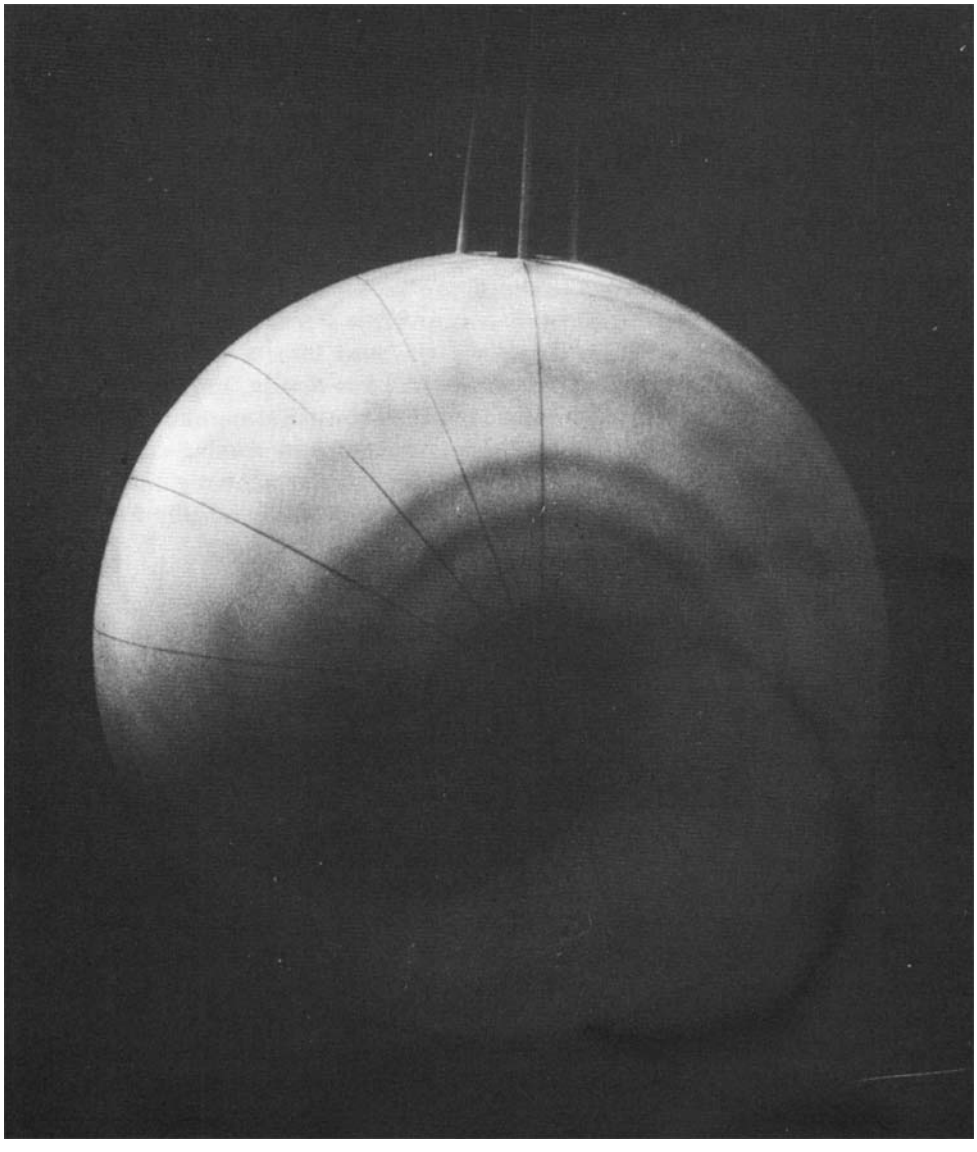

FIGURE 9. Streakline produced by dye released from the transverse pole, $\theta = \alpha = \frac{1}{2}\pi$, with 20 cm, 0.6 Hz waves progressing from left to right over a 20 cm sphere at mid-depth in 154 cm of water, $d_0/D = 0.359$.

the onset of separation, since $0.053 < d_0/D < 1.77$. Although the Reynolds number remained large, $118 < R^{(2)} < 34800$, mass transport in the boundary layer is independent of the low-Reynolds-number assumption. Furthermore, the steady streaming solutions inside the boundary layer, (5.9)–(5.11), remain valid for transitional waves, $0 < \tanh \frac{1}{2}kh < 1$. Therefore these observed drift rates are compared directly with the theoretical mass-transport velocity at the top of the boundary layer from (9.1). To avoid interference from the support strut situated on the upper

hemisphere, the mass-transport comparisons were made by averaging along the equator, $\alpha = 0$, over the lower hemisphere where

$$\frac{1}{\pi}\int_0^{\pi} \lim_{r\to 1} \boldsymbol{n}_\theta \cdot \langle \hat{\boldsymbol{u}}_{\mathrm{L}} \rangle_{\alpha=0}\, \mathrm{d}\theta = -\frac{39}{8}\,\frac{d_0}{D}\, w_{\mathrm{m}}. \tag{9.3}$$

Also included in figure 8 are values from Longuet-Higgins (1970), where dye was released near a circular cylinder executing circular oscillations in a basin of still fluid. It is found that the data fall close to the theory line of (9.3) until boundary-layer separation ensues at large amplitudes, as $d_0/D \to O(1)$. Mass transport is about the same near the surfaces of a cylinder or the vertical equator of a sphere as indicated by the theoretical steady-state results in figure 7.

While a net circumferential drift of dye around $\alpha = 0$ results from the Stokes drift and circulation streaming, figure 9 shows the end effects due to the acoustic streaming. Dye released from the transverse pole, $\alpha = \theta = \frac{1}{2}\pi$, migrates towards the vertical equator, $\alpha = 0$, under the influence of the acoustic streaming. As it proceeds away from the transverse pole, the dye streak develops increasing circulation from the circulation streaming. The combined action of the acoustic and circulation streaming results in the spiral streakline over the transverse hemisphere as portrayed in figure 9.

10. Forces and torques

The reaction forces and torques on the sphere are calculated from the fluid motion in the near field defined by the matched asymptotic solutions (2.8) and (2.13). To lowest order, the apportionment of these forces between normal stresses resulting from wave pressure and shear stresses developed in the boundary layer is calculated directly from the stress tensor in Lamb (1932, Art. 336) evaluated on the sphere. For the residual higher-order force components we employ a two-layer momentum survey equating the rate of change of fluid momentum within inner and outer concentric spherical control volumes to the sum of the forces acting on the boundaries of these volumes. The inner control volume is a thin spherical shell of fluid composed of the boundary layer. The outer control volume is the fluid outside the boundary layer extending to $\hat{r}/a \to \infty$. Matching momentum fluxes between the inner and outer control volumes and performing the tedious but straightforward integrations results in the following theoretical force components on a fixed sphere under a deep-water incident wave:

$$\begin{aligned}\hat{F}_x(\sigma\hat{t}) = {} & -\rho\tfrac{4}{3}\pi a^3\sigma u_{\mathrm{m}}\left[\frac{3}{2}+\frac{9}{4}\,\frac{\delta}{a}-\frac{d_0^2}{D^2}\left(\frac{27}{8}-0.15820R^{(2)}+0.8736\,\frac{\delta}{a}\right)\right]\sin\sigma\hat{t}\\ & +\rho\pi a^2 u_{\mathrm{m}}^2\left[3\left(\frac{2}{R^{(2)}}\right)^{\frac{1}{2}}\left(1+\frac{\delta}{a}\right)-\frac{d_0}{D}\left(\frac{3}{4}+0.32939R^{(2)}-14.5852\,\frac{\delta}{a}\right)\right]\cos\sigma\hat{t}\\ & +\rho\,\frac{d_0}{D}\,\frac{\delta}{a}\,\pi a^2 u_{\mathrm{m}}^2\,\frac{162}{5}\left(\frac{1}{\sqrt{2}}-\frac{1}{2}\right)(\cos 3\sigma\hat{t}-\sin 3\sigma\hat{t}) \quad (\tanh\tfrac{1}{2}kh\to 1),\end{aligned} \tag{10.1}$$

$$\hat{F}_z(\sigma\hat{t}) = \hat{F}_x(\sigma\hat{t}+\tfrac{1}{2}\pi), \tag{10.2}$$

$$\hat{F}_y(\sigma\hat{t}) = 0. \tag{10.3}$$

Under a plane shallow-water incident wave the force components are found to be

$$\hat{F}_x(\sigma\hat{t}) = -\rho\tfrac{4}{3}\pi a^3\sigma u_{\mathrm{m}}\left(\frac{3}{2}+\frac{9}{4}\,\frac{\delta}{a}-0.0099\,\frac{d_0^2}{D^2}\,\frac{\delta}{a}\right)\sin\sigma\hat{t}$$

$$+\rho\pi a^2u_{\mathrm{m}}^2\left[3\left(\frac{2}{R^{(2)}}\right)^{\frac{1}{2}}\left(1+\frac{\delta}{a}\right)-\frac{d_0}{D}\left(\frac{3}{2}+0.1005R^{(2)}-4.4867\,\frac{\delta}{a}\right)\right]\cos\sigma\hat{t}$$

$$+\rho\,\frac{d_0}{D}\,\frac{\delta}{a}\,\pi a^2u_{\mathrm{m}}^2\,\frac{54}{5}\left(\frac{1}{\sqrt{2}}-\frac{1}{2}\right)(\cos 3\sigma\hat{t}-\sin 3\sigma\hat{t})\quad(\tanh\tfrac{1}{2}kh\to 0), \tag{10.4}$$

$$\hat{F}_y(\sigma\hat{t}) = \hat{F}_z(\sigma\hat{t}) = 0. \tag{10.5}$$

As expected from flow symmetry, the transverse force $\hat{F}_y(\sigma\hat{t})$ is zero for both shallow- and deep-water limits.

Calculating $\boldsymbol{r}\times\boldsymbol{F}$ reveals that a torque τ also acts on the sphere about the horizontal transverse axis oy equal to

$$\hat{\tau} = \boldsymbol{n}_y\,\rho\pi a^3u_{\mathrm{m}}^2\tanh\tfrac{1}{2}kh\left\{\frac{\delta}{a}\,\frac{15}{8}+\frac{\delta}{a}\,\frac{d_0^2}{D^2}\,\frac{81}{16}\,[1-\tanh^2\tfrac{1}{2}kh]\right.$$

$$\left.+\frac{\delta}{a}\,\frac{d_0^2}{D^2}\,\frac{2187}{128}\left(\frac{1}{\sqrt{2}}-\frac{1}{2}\right)(\cos 2\sigma\hat{t}-\sin 2\sigma\hat{t})\right\}. \tag{10.6}$$

The torque in (10.6) has steady and second-harmonic components which vanish in the limit of a plane shallow-water wave, $\tanh\frac{1}{2}kh\to 0$.

The theoretical forces calculated in (10.1), (10.2) and (10.4) resemble a Fourier decomposition of Morison's equation based upon the periodic wave-particle velocity u_∞ (see Keulegan & Carpenter 1956). The bracketed terms appearing at the fundamental, σt, in (10.1) and (10.4) are indeed the time-independent virtual mass (inertia) and drag coefficients c_{m} and c_{f}. However, Morison's equation will not admit the presence of any mean or second-harmonic forces or torques when the fundamental oscillation is periodic, $\langle u_\infty\rangle = 0$.

The leading term of the drag coefficient in (10.1) and (10.2) is identical with the Stokes pendulum (Stokes 1851; Lamb 1932, Art. 356). A $-\frac{1}{2}$-power dependence on the Reynolds number is a hallmark of laminar boundary layers, either steady or periodic. Two-thirds of this leading-order drag-coefficient term is due to boundary-layer shear stresses, while the remaining one-third is the in-phase resultant of the pressure from the phase-shifted secondary wave radiation. The $O((\delta/a)\,(R^{(2)})^{-\frac{1}{2}})$ drag-coefficient term is also the same as that given in the Stokes-pendulum solution, and results from the shear stresses of the $O(\delta/a)$ viscous correction to the boundary-layer profile.

The $O(d_0/D)$ correction to the drag coefficient in (10.1) and (10.4) is a new result, which Stokes' analysis could not give because of neglect of nonlinear terms. This correction is due to the periodic movement of the steady x-directed momentum from the diffusive acoustic streaming by the vibrations of the $O(1)$ wave motion. The acoustic-streaming field thereby functions as a source of x-directed momentum. Consequently, this effect could be referred to as 'acoustic thrust'. The $O(d_0/D)$ correction to the drag coefficient from acoustic thrust is twice as large for the plane shallow-water wave solution (10.4). This can be explained by the different alignments and flow directions of the diffusive acoustic-streaming field between the deep- and shallow-water extremes. Since inflow and outflow regions are partitioned about

$\theta' = 55°$ and $\theta = 55°$ in deep- and shallow-water extremes respectively (see (7.15) and (7.16)), it follows that radial outflow in the deep-water solution must have less x-directed momentum than the axial outflow in the shallow-water solution. Therefore the alignment and flow direction of the shallow-water diffusive acoustic-streaming field makes it a more effective source of x-directed momentum.

The advective correction on the acoustic streaming fields in both deep- and shallow-water extremes intensified the outflow (see figures 4 and 6), thereby increasing the x-directed steady momentum available for transport by the $O(1)$ periodic flow. Consequently there are additional $O((d_0/D)\,R^{(2)})$ corrections to the drag coefficient in (10.1) and (10.4) resulting from acoustic thrust. The correction at this order is stronger in the deep-water case because outflow has been enhanced more by the action of centrifugal pumping from the circulation-streaming field.

The $O((d_0/D)\,(\delta/a))$ corrections to the drag coefficient in (10.1) and (10.4) result from several different higher-order momentum fluxes. Both deep- and shallow-water solutions receive contributions from the transport of $O(1)$ momentum by the second-harmonic wave radiation. These momentum fluxes give rise to forces at the fundamental, σt, and at the third harmonic, $3\sigma t$. However, the deep-water solution receives an additional contribution from the outward flux of circulation-streaming momentum by the phase-shifted secondary wave radiation. This momentum flux is analogous to induced drag on a three-dimensional lifting body. There are additional induced drag contributions from flux terms $O((d_0^2/D^2)\,a^2u_m^2)$, which unfortunately become vanishingly small as $r\to\infty$. A similar difficulty was encountered in wing theory (Prandtl & Tietjens 1934) and was resolved by lifting-line theory (see Van Dyke 1975). Since the aspect ratio of a sphere is not large ($4/\pi$), the error in calculating induced drag by lifting-line theory is unacceptably large, $O(\frac{1}{16}\pi^2)$.

The leading terms of the virtual-mass coefficient through $O(\delta/a)$ in (10.1) and (10.4) would be the same as those in the Stokes-pendulum solution if the fluid–pendulum system were oscillated contrary to the pendulum motion to yield a sphere at rest in an oscillatory fluid. Two-thirds of the $O(\delta/a)$ correction to the inviscid value of $\frac{3}{2}$ is due to the additional mass of fluid entrained by the retarded boundary-layer flow. The remaining one-third of the $O(\delta/a)$ correction is the in-quadrature pressure resultant of the phase-shifted secondary wave radiation.

An interesting new result in the deep-water wave-force solutions (10.1) and (10.2) is the presence of the $O(d_0^2/D^2)$ corrections, which act to diminish the virtual-mass (inertia) coefficient c_m. These corrections are due to the inertia of the circulation streaming, appearing in the fluid both as a momentum flux far away in the interior, and from the boundary layer. These momentum fluxes result in a rotary force F_1 on the sphere, acting normally to the instantaneous $O(1)$ velocity u_∞, as given by

$$\hat{\boldsymbol{F}}_1 = \rho\tfrac{4}{3}\pi a^2\hat{\boldsymbol{\Omega}}_0 \times \hat{\boldsymbol{u}}_\infty \left(1 - 0.04687R^{(2)} + \frac{7}{4}\,\frac{\delta}{a}\right). \tag{10.7}$$

The Reynolds-number correction in (10.7) results from the advective correction to the circulation streaming, and is analogous to the reduction in lift on a three-dimensional wing whose aspect ratio is made small.

The $O((d_0/D)^2\,(\delta/a))$ corrections to the virtual-mass coefficient found in both the deep- and shallow-water solutions (10.1) and (10.4) are independent of the presence of circulation. They are instead the in-quadrature resultant of $O(1)$ momentum being transported by the phase-shifted vibrations of the second harmonic wave. The

correction is larger for the deep-water case because the second-harmonic oscillation is progressive around the sphere and thereby transports more $O(1)$ momentum than the standing second-harmonic oscillation found for the shallow-water solution.

11. Conclusions

(*A*) Diffusive solutions to the vorticity-transport equations remain sufficiently well behaved in three dimensions to iterate for advective corrections at low Reynolds numbers in periodic flow.

(*B*) These advective corrections exhibit certain high-Reynolds-number-like flow features. Among these are stationary steady eddies in the shallow-water case, and a radial jet in the deep-water case.

(*C*) Resistance coefficients at low Reynolds numbers vary with both frequency- and amplitude-dependent parameters. A third-harmonic force and steady and second-harmonic torques arise which cannot be approximated by Morison's equation.

This research was sponsored by the Office of Naval Research Code 421 under contract with the Scripps Institution of Oceanography, University of California. The authors particularly credit the contribution of Mr George Halikas, who passed away before this work could be completed.

REFERENCES

ANDREWS, D. G. & MCINTYRE, M. E. 1978 An exact theory of nonlinear waves on a Lagrangian-mean flow. *J. Fluid Mech.* **89**, 609–647.

BATCHELOR, G. K. 1967 *An Introduction to Fluid Dynamics*. Cambridge University Press.

BICKLEY, W. G. 1938 The secondary flow due to a sphere rotating in a viscous fluid. *Phil. Mag.* (7) **25**, 746–752.

DUCK, P. W. & SMITH, F. T. 1979 Steady streaming induced between oscillating cylinders. *J. Fluid Mech.* **91**, 93–107.

ECKART, C. 1948 Vortices and streams caused by sound waves. *Phys. Rev.* **73**, 68–76.

GOLDSTEIN, S. (ed.) 1938 *Modern Developments in Fluid Dynamics*. Oxford University Press.

HAVELOCK, T. H. 1954 The forces on a submerged body moving under waves. In *The Collected Papers of Sir Thomas Havelock on Hydrodynamics*; ONR/ACR-103, pp. 590–596.

HILDEBRAND, F. B. 1963 *Advanced Calculus for Applications*. Prentice-Hall.

HOWARTH, L. 1951 Note on the boundary layer on a rotating sphere. *Phil. Mag.* (7) **42**, 1308–1315.

HUNT, J. N. & JOHNS, B. 1963 Currents induced by tides and gravity waves. *Tellus* **15**, 343–354.

KEULEGAN, G. H. & CARPENTER, L. H. 1956 Forces on cylinders and plates in an oscillating fluid. *Nat. Bur. Stand.* 4821.

LAMB, H. 1932 *Hydrodynamics*. Dover.

LAMOURE, J. & MEI, C. C. 1977 Effects of horizontally two-dimensional bodies on the mass transport near the sea bottom. *J. Fluid Mech.* **83**, 415–433.

LONGUET-HIGGINS, M. S. 1953 Mass transport in water waves. *Phil. Trans. R. Soc. Lond.* A **245**, 535–581.

LONGUET-HIGGINS, M. S. 1970 Steady currents induced by oscillations around islands. *J. Fluid Mech.* **42**, 701–720.

MORSE, P. M. & FESHBACH, H. 1953 *Methods of Theoretical Physics*, vols. I and II. McGraw-Hill.

PRANDTL, L. & TIETJENS, O. G. 1934 *Applied Hydro and Aeromechanics*. McGraw-Hill.

RAYLEIGH, LORD 1876 On waves. *Phil. Mag.* (5) **1**, 257–259.

RILEY, N. 1967 Oscillatory viscous flows, review and extension. *J. Inst. Maths Applics* **3**, 419–434.

RUBINOW, S. I. & KELLER, J. B. 1961 The transverse force on a spinning sphere moving in a viscous fluid. *J. Fluid Mech.* **11**, 447–459.

SCHLICHTING, H. 1932 Berechnung ebener periodischer Grenzschichtströmungen. *Phys. Z.* **33**, 327–335.

STOKES, G. G. 1851 On the effect of internal friction of fluids on the motion of pendulums. *Trans. Camb. Phil. Soc.* **9**, 25–106.

VAN DYKE, M. 1975 *Perturbation Methods in Fluid Mechanics.* Parabolic.